

Coarse-graining and designing liquids with the Ornstein-Zernike equation and machine learnt closures

Rhys E. A. Goodall and Alpha A. Lee*

Cavendish Laboratory, University of Cambridge, Cambridge CB3 0HE, UK

E-mail: aal44@cam.ac.uk

Abstract

A key challenge for soft materials design and coarse-graining simulations is determining interaction potentials between components that would create the desired condensed phase structure. In theory, the Ornstein-Zernike framework provides an elegant route for solving this inverse problem. The missing link is the so-called closure relation. Pioneering work in liquid state theory derived analytical closures, but they are approximations valid only for specific classes of interaction potentials. In this paper, we combine the physics of liquid state theory with deep learning. We use machine learning to infer a closure directly from simulation data. Our resulting closure is broadly accurate across the space of interaction potentials. We show that our approach solves the inverse problem in simple liquids with an accuracy higher than commonly used closures, as well as tackles prototypical problems in fitting coarse-grained simulations.

Introduction

A central question in soft matter pertains to the inverse problem of determining an interaction potential between building blocks, e.g. colloids or molecules, that results in a target pair

correlation function in the condensed phase. Applications of this inverse problem abound in disparate fields. For instance, molecular interactions can be optimised to yield porous structures in a liquid^{1,2} which is crucial to chemical processes such as gas separation and storage. More generally, a key question in soft materials design is determining the interaction potentials between particles that would create desired structures through self-assembly^{3,4}, as well as to optimise the kinetics of such assembly process⁵. This inverse problem is also important to coarse-graining, a technique which aims to speed up molecular simulations by lumping together degrees of freedom which evolve over a smaller lengthscale/faster timescale than the phenomenon under study⁶⁻⁸. An important step in coarse-graining involves finding effective interparticle interactions between those coarse-grained “beads” to reproduce the structure of the full system.

However, although the forward problem of predicting condensed phase structure given a set of interactions can be tackled with standard methods such as molecular dynamics or Monte Carlo simulation, the inverse problem remains computationally challenging. Typically techniques such as Iterative Boltzmann Inversion⁹, which involves an iterative optimisation loop where each optimisation step requires a converged molecular dynamics simulation of the coarse-grained system, are employed.

Nonetheless, in theory, a rigorous framework in statistical physics known as the Ornstein-Zernicke equation¹⁰ provides a direct and computationally efficient framework to solve this inverse problem without any simulations. The missing link is the so-called closure equation. Although many analytical closures have been developed over the years, they are valid only for specific classes of interaction potentials.

In this paper, we depart from conventional wisdom and use machine learning to infer a closure directly from simulation data. We will first discuss the Ornstein-Zernicke framework and our machine learning methodology. We will then show that our machine-learned closure is accurate for across the space of interaction potentials. We demonstrate that our closure solves the inverse problem in simple liquids with an accuracy higher than commonly used

closures, as well as tackles prototypical problems in fitting coarse-grained simulations.

The Ornstein-Zernike Equation

The Ornstein-Zernike equation states that the total correlation function, $h(r)$, for an isotropic fluid of density ρ can be decomposed into direct correlations and indirect correlations between particles:

$$h(r_{12}) = c(r_{12}) + \rho \int c(r_{13})h(r_{32})dr_3 \quad (1)$$

Where r_{ij} denotes the pairwise distance between the i^{th} and j^{th} particles. In a isotropic system the average environments of different particles of the same species are the same and so from here onward we drop these indices for clarity. This equation defines the direct correlation function, $c(r)$. $h(r)$ is related to the more commonly used radial distribution function by $h(r) = g(r) - 1$. The second term in the Ornstein-Zernike equation is the convolution of $h(r)$ and $c(r)$, therefore taking the Fourier transform yields an algebraic equation in q -space.

$$H(q) = C(q) + \rho H(q)C(q) \quad (2)$$

This equation can be broken apart and re-written it in terms of the static structure factor, $S(q)$. Doing so establishes a straightforward link between the formalism in q -space and readily available experimental information in the form of the static structure factor – real experiments more often tend to obtain structural information in the form of the structure factor via scattering experiments than they attempt to measure the particle positions and calculate the radial distribution function directly.

$$H(q) = \frac{1}{\rho} \left(S(q) - 1 \right) \quad (3)$$

$$C(q) = \frac{1}{\rho} \left(1 - \frac{1}{S(q)} \right) \quad (4)$$

To solve the inverse design problem of determining the potential, $\phi(r)$, that gives rise to a structure a second equation, a closure relationship, coupling $h(r)$ and $c(r)$ with $\phi(r)$, is needed. The generally accepted form of the closure function is:

$$h(r) + 1 = \exp(-\beta\phi(r) + \gamma(r) + B(r)) \quad (5)$$

where $B(r)$ is the bridge function and $\gamma(r) = h(r) - c(r)$ is the indirect correlation function. Whilst diagrammatic expansions exist that define $B(r)$, they do so as an infinite and slowly converging series¹¹. As such, for practical applications it is necessary to use an approximation for the bridge function to close the system of equations. Traditionally, closure relationships approximate $B(r)$ with a functional in terms of $\gamma(r)$. The most commonly used are the Hyper-netted Chain approximation (HNC)¹², $B(r) = 0$, and the Percus-Yevick approximation (PY)¹³, $B(r) = \ln(1 + \gamma(r)) - \gamma(r)$. The HNC closure is the most generally applicable being well suited for long-range potentials whilst the PY closure works well for short-range, purely repulsive systems.

Learning Generally Applicable

Closure Relationships

Machine learning offers an ever improving suite of powerful tools that can be used for function approximation. Given this we are no longer tied to analytically tractable closures such as HNC or PY. However, before such techniques can be applied it is important to consider whether the input features given to the model might contain sufficient information to determine the system. From a theoretical standpoint $B(r)$ can be expanded as an infinite series in $\gamma(r)$ ¹⁴:

$$B(r) = \frac{\bar{F}_3}{2!} \gamma^2(r) + \frac{\bar{F}_4}{3!} \gamma^3(r) + \dots \quad (6)$$

where the average modification functions, \bar{F}_n , are dependant on the density, ρ , and the temperature, T . By unit analysis the bridge function can only be expressed in terms of dimensionless reduced quantities ρ^* and T^* . However, for complicated pairwise potentials, where multiple length and energy scales are required to define the system, comparable reduced quantities are ill-defined preventing formulation of a truly general closure in terms of $\gamma(r)$ only. However, this knowledge suggests that there is scope to improve upon currently closures by including additional input features that allow us to recover the degree of freedoms corresponding to the reduced temperatures and densities. This argument is consistent with the boost in performance observed from introducing switching functions in both the Rogers-Young and Zerah-Hansen closures^{15,16}. However, unlike with these approaches where the switching length-scale is fitted to match thermodynamic properties, any additional input features for a learnt closure must be constructed without prior knowledge of the target system.

From Equation 1 we see that we can extract the density of the system if given both $h(r)$ and $c(r)$. This suggests that together $h(r)$ and $c(r)$ are more informative than $\gamma(r)$. Therefore, closures expressed in the form $B(r) = B(h(r), c(r), \dots)$ may be able to be applied to a wider variety of systems.

The next additional feature we identify comes from considering that such liquid systems exist in an equilibrium defined by detailed balance. Therefore, drawing inspiration from the fluctuation-dissipation theorem we define an additional feature of the form:

$$\chi(r) = \frac{\langle (g(r))^2 \rangle - \langle g(r) \rangle^2}{\langle g(r) \rangle} \times \sqrt{N}, \quad (7)$$

where the variance of $g(r)$ is computed between de-correlated samples obtained by applying the Flyvbjerg-Petersen blocking algorithm to samples of $g(r)$ from the simulation¹⁷. In order

to remove the dependence of the variance on the number of particles under observation, N , we scale by \sqrt{N} . While readily accessible in simulation studies the number of particles is harder to obtain in physical experiments - doing so depends on accurate knowledge of both the density (already necessary to obtain $h(r)$ and $c(r)$ from $S(q)$) and the scattering volume of the beam. However, this feature is highly correlated to the apparent 'softness' of the potential's divergence and therefore contains important information if our learnt closure is expected to perform well over a large variety of potentials.

The next extension we explore is the inclusion of non-local information into the closure. To do this we opt to include $\gamma'(r)$ rather than $h'(r)$ and $c'(r)$ as the latter contain sharp jumps around the first co-ordination shell that cancel each other out in $\gamma'(r)$. Such sharp jumps are undesirable as they provide artefacts to which the model can overfit on in the training data leading to poor generalisation performance in downstream applications. The naive definition of the gradient is system specific depending on the length-scales of the system under investigation and therefore not necessarily compatible with construction of a universal closure. To resolve this problem we define the natural length-scale of the systems under study as the radius of the first co-ordination shell. Having a fixed reference allows the gradients to be defined in a self-consistent manner making this feature amenable to use in a learnt closure.

Methods

Data Generation

Despite remarkable successes, most machine learning approaches are essentially powerful interpolation frameworks. Therefore, in order to infer a generally applicable closure we need to explore a wide variety of the possible interaction potentials. We investigated thirteen different interaction potentials, grouped loosely into four classes: Hard-Sphere - potentials containing strong divergences that prevent particles from overlapping, Core-Softened - hard-

sphere models where a repulsive plateau is added before the divergence to introduce complex multi-lengthscale structure, Soft-Sphere - weakly divergent systems analogous to hard-sphere systems, and Soft-Core - potentials that do not diverge and allow particles to overlap. We will refer to Hard-Sphere and Core-Softened potentials as hard potentials and Soft-Sphere and Soft-Core potentials as soft potentials. For each of these potentials the molecular dynamics package ‘ESPReso’^{18,19} was used to determine $h(r)$ and $S(q)$ for systems particles at various temperatures and densities with the box size being held constant. Full details of the functional forms for the potentials investigated and simulation setup are available in the SI.

Fitting a Machine Learning model

Unlike the construction of the feature set the selection of a model architecture is dominated by practical rather than physical constraints. Here we have a limited feature set but can generate a large number of data-points. Therefore, kernel models such as Support Vector Machines, Kernel Ridge Regression or Gaussian Processes are undesirable as the kernel memory requirement scales as $O(n^2)$ where n is the number of data points. Random Forests are another commonly used Machine Learning model however, it is explicate in their construction that they are unable to extrapolate which makes them undesirable for this application. Neural networks are a high-flexible modelling approach that makes use of stochastic gradient descent to train a parameterised model constructed as a sequence of affine transformations and non-linearities (activation functions). While they are perhaps harder to interpret than the previously highlighted models they do not suffer from the same limitations. For our work we make use of a very simple fixed architecture - a pyramidal multi-layer perception with [256, 128, 64, 32] neurons in each of its layers and ‘ReLU’ activation functions. We use a weighted L2 loss function as we have explicate access to the variance in our samples of $B(r)$. The Adam optimiser is used with default parameters and the networks are trained for 200 epochs.

Results and Discussion

Testing the feature set

To test our feature set we train several models using different combinations of features: 1) B_{GA} - a closure just in terms of $\gamma(r)$ as has been common with analytical closures in the field, 2) B_{LA} - a closure in terms of $h(r)$ and $c(r)$, 3) B_{FA} - a closure including $h(r)$, $c(r)$ and $\chi(r)$, and 4) B_{NLA} - a non-local closure that takes $\gamma'(r)$ and all the local features as inputs.

We assess the performance of our learnt closures and HNC on a randomly sampled test set comprising 20% of the simulation data that was withheld when training the learnt closures. The learnt closure based on just the indirect correlation function, B_{GA} , has a negative R^2 implying that it is worse than predicting a constant value (i.e. HNC). However, Table 1 shows that as we extend the feature set to include additional physically motivated features the learnt closures offer rapidly improving performance compared to HNC. Using the full feature set, B_{NLA} , leads to a very strong correlation between the learnt closure’s predictions and the ground truth with a R^2 value of 0.835. Fig 1 shows that this improved performance is due to the ability of the learnt closure to correctly predict large negative values of the bridge function. Physically this corresponds to the learnt closures being able to capture the strongly correlated physics in the region around the first co-ordination shell. This is the region where the failures of traditional closures are most pronounced.

Table 1: Performance of learnt closures with different feature sets and HNC on a randomly held-out test set.

Closure	R^2	RMSE	MAE
HNC	0.000	0.104	0.028
$B_{GA} = B(\gamma)$	-1.523	0.091	0.021
$B_{LA} = B(h, c)$	0.201	0.073	0.017
$B_{FA} = B(h, c, \chi)$	0.543	0.058	0.013
$B_{NLA} = B(h, c, \chi, \gamma')$	0.835	0.038	0.009

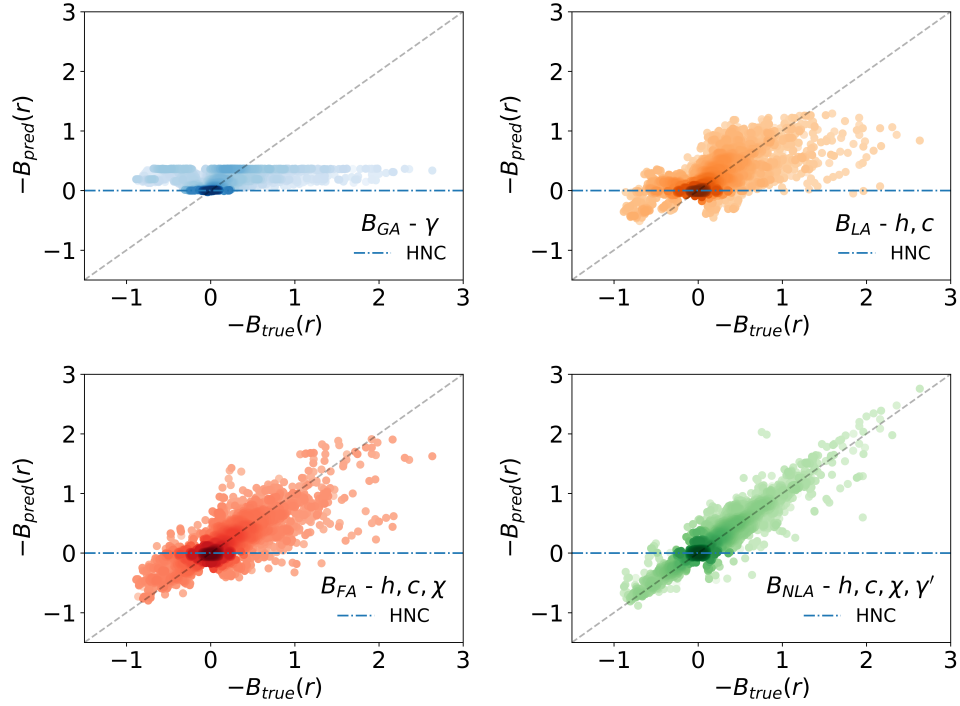


Figure 1: The figure shows parity plots between the predictions of the closures trained using different feature sets. The points are shaded according to the log of the density of points. For all the learnt closures we see a dark spot at the origin which correspond to the networks learning the correct far field behaviour. We see that as we extend the feature set we get better at predicting the value of bridge function, $B(r)$.

Generalisation performance across potential classes

The above results show that learnt closures exhibit far greater universality than previous analytical closures, such as HNC or PY, when trained and tested on a diverse selection of different potentials. However, an interesting question is whether this is true generalisation performance that would extend even further to out-of-training-distribution regimes. We can explore this scenario by looking at how learnt closures perform when trained on restricted classes of potential. We train two learnt closures using the full feature set, one on only hard potentials (*HardNet*) and a second on only soft potentials (*SoftNet*) (Fig 2). We see that when out-of-training-distribution generalisation performance is tested, our learnt closures are less accurate in their out-of-training-distribution regimes. Our analysis on generalisation performance suggest that it would not be reasonable to apply our learnt closures in applications involving qualitatively different potentials (e.g. charged liquids, where the correlation length-scales are much longer) without first extending the training data to also include such systems.

Coarse-graining with machine learnt closures

To test the potential benefits of using a learnt closure in downstream applications, we examine the prototypical task of coarse graining the solvent degrees of freedom in a two component solvent-solute mixture. The challenge is determining the effective solute-solute interaction such that the resulting solute-only (one-component) simulation reproduces the solute pair distribution function of the underlying solute-solvent (two-component) system. Such inverse problems are usually solved using iterative methods such as Iterative Boltzmann Inversion (IBI) and multi-state variants thereof^{20,21}. Recent work has extended IBI to make use of the Ornstein-Zernike framework in Iterative Ornstein-Zernike Inversion (IOZI)²² where the iteration scheme relies on the use of a closure approximation to close the equations. Both processes work by running forward simulations to find the liquid structure that results from a given test potential. The resulting structures are then used to iteratively update the test

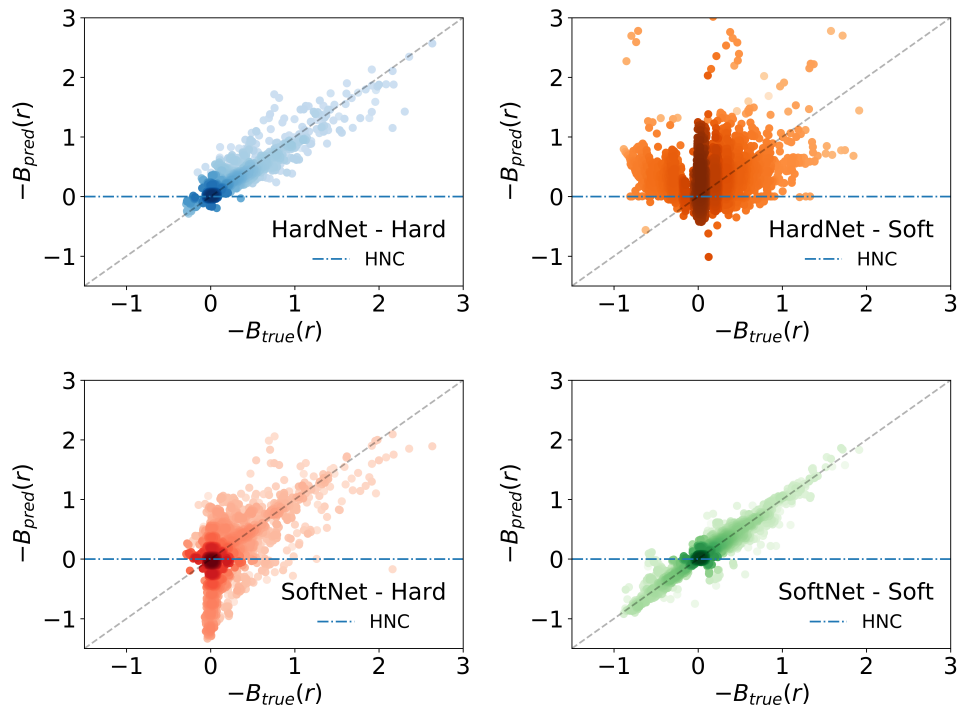


Figure 2: This figure shows the limitations of learnt closures to generalise to regimes not included in their training. The points are shaded according to the log of the density of points. While we see strong performance for both *HardNet* and *SoftNet* when tested on similar potentials as those used to train them, they are much less predictive of their out-of-training-distribution regimes. This motivates the need to attempt to construct a training set such that all likely applications of the model fall within the interpolative regime of the learnt closure.

potential in order to minimise deviations between the observed structure and the desired structure according to the general update rule:

$$\begin{aligned} \phi_{n+1}(r) = & \phi_n(r) + k_b T \ln \left(\frac{g_n(r)}{g^*(r)} \right) + h^*(r) - h_n(r) \\ & - c^*(r) + c_n(r) + \hat{B}^*(r) - \hat{B}_n(r) \end{aligned} \quad (8)$$

Where $\hat{B}^*(r)$ denotes the best estimate of $B^*(r)$ given some closure. IBI corresponds to keeping just the first two terms on the right hand-side of this iteration scheme. All of these methods rely on making some initial estimate for the potential, for IBI this is typically:

$$\phi_1(r) = -k_b T \ln(g^*(r)) \quad (9)$$

whilst for IOZI the initial estimate is:

$$\phi_1(r) = -k_b T \ln(g^*(r)) + h^*(r) - c^*(r) + \hat{B}^*(r) \quad (10)$$

Improved initial estimates have the potential to significantly speed up the convergence of the iteration process. Indeed, a true closure to the Ornstein-Zernike formalism, one yielding the correct $B^*(r)$, would converge to the true solution with one iteration. As such, a valid comparison of the different approaches can be made purely on how well the initial estimate reproduces a liquid structure that matches the target. Fig 1 shows that our learnt closures perform much better at predicting $B(r)$ in the regions where HNC fails, suggesting that using the learnt closures for producing initial estimates for the interaction potential in coarse graining tasks is a highly promising application.

Our toy problem consists of equal quantities of two species of Lenard-Jones particles with relative radii of σ and 0.5σ respectively (Full details in SI) – one could imagine this setup to model the larger particles “solvated” in a bath of smaller particles. We measure

$g^*(r)$ and $S^*(q)$ between the larger species only and use this information to extract $c^*(r)$ and estimate $\hat{B}_{NLA}^*(r)$. As we generate the estimate of the bridge function in a point-wise manner, the resulting potential contains some high frequency noise terms which create large and unphysical forces when we take the gradient. To deal with this we apply a quadratic Savitzky-Golay filter to the estimated bridge function in order to obtain a smooth potential and, as a consequence, well behaved forces²³.

Table 2: Performance of closures and HNC on the test set.

$\phi_1(r)$ Initialisation	MAE	RMSE	W
IBI	0.0062	0.063	0.240
HNC	0.0008	0.041	0.045
NLA	0.0005	0.031	0.030

To quantify the downstream performance of our closure, we report the RMSE and MAE metrics as well as the Wasserstein or 'earth-movers' distance, W, between the target particle density, $r^2g^*(r)$, and the density that results from our initialisation, $r^2g_1(r)$. This measure is directly related to the amount by which particles would need to be moved to recover the target density. According to these metrics using the learnt closure gives a much better initial estimate than the other approaches. We can probe this further by looking at the recovered structures in Fig 3. We see that whilst the learnt closure overestimates the height of the principal peak, it does a much better job than either the IBI or HNC initialisation at matching the complex step like structure of the $g^*(r)$ around 1.6σ , therefore providing a better overall result.

Conclusions

In this work we demonstrate that machine learning is an effective tool for tackling inverse problems in soft matter. We use the physics-derived framework of Ornstein-Zernike theory but employ machine learning to parameterise the closure relationship using physical descriptors of the pair correlation function. Our approach is accurate in regions where traditional

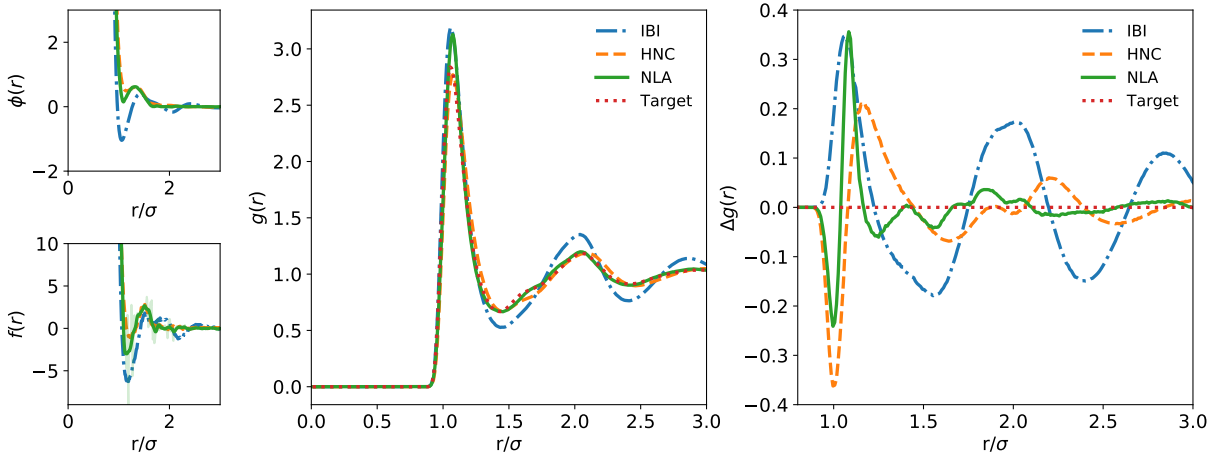


Figure 3: The small plots on the left hand side show the initial estimates potential for the potential and force using IBI, HNC and our full learnt closure (NLA). In order to obtain well-behaved forces a Savitzky-Golay filter has been used to smooth the estimated bridge function - the original noisy results are also plotted alongside the smoothed results with high transparency. The central plot shows the resulting $g(r)$ curves for each of these initialisation as well as the original target distribution. Both IBI and our closure result in distributions that overestimate the height of the principal peak while HNC underestimates the peak. Beyond the principle peak the learnt closure provides a much closer match to the target distribution as can be seen clearly in the rightmost plot, which shows the difference between the resulting and target distributions.

analytical approximations tend to fail. We show that learnt closures are able to predict the bridge function to sufficient accuracy to have meaningful benefits in scientifically interesting downstream applications, such as the coarse-graining of complicated multi-species systems. We envisage that future work will be able to generalise and extend upon the approach adopted here to obtain increased efficacy closures in a wide variety of systems to which the Ornstein-Zernike framework has been applied.

More broadly, our work contributes to the growing literature on exploring how to combine the best of physics-based models and machine learning approaches. Whilst many theoretical frameworks in chemical sciences are elegant and exact, the implementation of those frameworks typically require approximations and fitted functions. This is particularly true in soft matter where timescale and lengthscale challenges necessitate the use of creative approximations. We believe advances abound in approaches that leverage the overall physics framework, but employ machine learning to determine those fitting functions directly from data.

Conflicts of interest

There are no conflicts to declare.

Acknowledgement

REAG and AAL thank the Winton Programme for the Physics of Sustainability at the University of Cambridge for funding. Part of this research was performed while REAG was visiting the Institute for Pure and Applied Mathematics (IPAM), which is supported by the National Science Foundation (Grant No. DMS-1440415).

Supporting Information Available

The following files are available free of charge.

The following supporting files are available:

- supporting.pdf: documents the interaction potentials and simulation setup used for the experiments detailed in the paper.

References

- (1) Giri, N.; Del Pópolo, M. G.; Melaugh, G.; Greenaway, R. L.; Rätzke, K.; Koschine, T.; Pison, L.; Gomes, M. F. C.; Cooper, A. I.; James, S. L. Liquids with permanent porosity. *Nature* **2015**, *527*, 216–220.
- (2) Lindquist, B. A.; Jadrich, R. B.; Truskett, T. M. Assembly of nothing: Equilibrium fluids with designed structured porosity. *Soft matter* **2016**, *12*, 2663–2667.
- (3) Jadrich, R.; Lindquist, B.; Truskett, T. Probabilistic inverse design for self-assembling materials. *The Journal of Chemical Physics* **2017**, *146*, 184103.
- (4) Sherman, Z. M.; Howard, M. P.; Lindquist, B. A.; Jadrich, R. B.; Truskett, T. M. Inverse methods for design of soft materials. *The Journal of Chemical Physics* **2020**, *152*, 140902.
- (5) Miskin, M. Z.; Khaira, G.; de Pablo, J. J.; Jaeger, H. M. Turning statistical physics models into materials design engines. *Proceedings of the National Academy of Sciences* **2016**, *113*, 34–39.
- (6) Kmiecik, S.; Gront, D.; Kolinski, M.; Wieteska, L.; Dawid, A. E.; Kolinski, A. Coarse-grained protein models and their applications. *Chemical reviews* **2016**, *116*, 7898–7936.

- (7) Marrink, S. J.; Risselada, H. J.; Yefimov, S.; Tieleman, D. P.; De Vries, A. H. The MARTINI force field: coarse grained model for biomolecular simulations. *The journal of physical chemistry B* **2007**, *111*, 7812–7824.
- (8) Brini, E.; Algaer, E. A.; Ganguly, P.; Li, C.; Rodriguez-Roper, F.; van der Vegt, N. F. Systematic coarse-graining methods for soft matter simulations—a review. *Soft Matter* **2013**, *9*, 2108–2119.
- (9) Schommers, W. Pair potentials in disordered many-particle systems: A study for liquid gallium. *Physical Review A* **1983**, *28*, 3599.
- (10) Ornstein, L.; Zernike, F. Accidental deviations of density and opalescence at the critical point of a single substance. *Proc. Akad. Sci.* **1914**, *17*, 793.
- (11) Hansen, J.; McDonald, I. *Theory of Simple Liquids*; Elsevier Science, 2006.
- (12) Morita, T. Theory of Classical Fluids: Hyper-Netted Chain Approximation, Formulation for a One-Component System. *Progress of Theoretical Physics* **1958**, *20*, 920–938, DOI: 10.1143/PTP.20.920.
- (13) Percus, J. K.; Yevick, G. J. Analysis of Classical Statistical Mechanics by Means of Collective Coordinates. *Phys. Rev.* **1958**, *110*, 1–13, DOI: 10.1103/PhysRev.110.1.
- (14) Lee, L. *Molecular Thermodynamics of Electrolyte Solutions*; World Scientific Publishing Company, 2008.
- (15) Rogers, F. J.; Young, D. A. New, thermodynamically consistent, integral equation for simple fluids. *Phys. Rev. A* **1984**, *30*, 999–1007, DOI: 10.1103/PhysRevA.30.999.
- (16) Zerah, G.; Hansen, J. Self consistent integral equations for fluid pair distribution functions: Another attempt. *The Journal of Chemical Physics* **1986**, *84*, 2336–2343, DOI: 10.1063/1.450397.

- (17) Flyvbjerg, H.; Petersen, H. G. Error estimates on averages of correlated data. *The Journal of Chemical Physics* **1989**, *91*, 461–466.
- (18) Limbach, H. J.; Arnold, A.; Mann, B. A.; Holm, C. ESPResSo – An Extensible Simulation Package for Research on Soft Matter Systems. *Comp. Phys. Comm.* **2006**, *174*, 704–727.
- (19) Arnold, A.; Lenz, O.; Kesselheim, S.; Weeber, R.; Fahrenberger, F.; Roehm, D.; Košovan, P.; Holm, C. ESPResSo 3.1 — Molecular Dynamics Software for Coarse-Grained Models. *Meshfree Methods for Partial Differential Equations VI*. 2013; pp 1–23, DOI: 10.1007/978-3-642-32979-1_1.
- (20) Reith, D.; Pütz, M.; Müller-Plathe, F. Deriving effective mesoscale potentials from atomistic simulations. *Journal of computational chemistry* **2003**, *24*, 1624–1636.
- (21) Moore, T. C.; Iacovella, C. R.; McCabe, C. Derivation of coarse-grained potentials via multistate iterative Boltzmann inversion. *The Journal of chemical physics* **2014**, *140*, 06B606_1.
- (22) Heinen, M. Calculating particle pair potentials from fluid-state pair correlations: Iterative ornstein–zernike inversion. *Journal of computational chemistry* **2018**, *39*, 1531–1543.
- (23) Savitzky, A.; Golay, M. J. Smoothing and differentiation of data by simplified least squares procedures. *Analytical chemistry* **1964**, *36*, 1627–1639.

Supplementary Information: Coarse-graining and designing liquids with the Ornstein-Zernike equation and machine learnt closures

Rhys E. A. Goodall and Alpha A. Lee*

Cavendish Laboratory, University of Cambridge, Cambridge CB3 0HE, UK

E-mail: aal44@cam.ac.uk

Potential Systems

Hard-Sphere Potentials:

- Lennard Jones 6-12 (LJ)

$$\phi(r) = 4\epsilon \left(\left(\frac{\sigma}{r} \right)^{12} - \left(\frac{\sigma}{r} \right)^6 \right) \quad (1)$$

Lennard Jones is the classical potential used when simulating simple systems. It encapsulates two key effects, hard-sphere repulsion and long range Van der Waals attraction.

- Morse

$$\phi(r) = \epsilon(\exp[-2\alpha(r - r_{min})] - 2\exp[-\alpha(r - r_{min})]) \quad (2)$$

The Morse potential is qualitatively similar to LJ but allows slightly more freedom to tune the shape of the minimum. It is often used to model the inter-atomic interactions

inside diatomic molecules such as N_2 .

- Generalised Pseudo-Hard-Sphere

$$\phi(r) = \frac{\lambda_r}{\lambda_r - \lambda_a} \left(\frac{\lambda_r}{\lambda_a} \right)^{\frac{\lambda_r}{\lambda_r - \lambda_a}} \epsilon \left(\left(\frac{\sigma}{r} \right)^{\lambda_r} - \left(\frac{\sigma}{r} \right)^{\lambda_a} \right) \quad (3)$$

The Mei Potential is a generalised form of LJ that offers more freedom to tune the shape of the potential.

The Weeks-Chandler-Andersen (WCA) potential¹ is defined by truncating and shifting the LJ potential at its minimum, the resulting potential is purely repulsive. We have constructed the equivalent to WCA for the generalised Mei potential allowing us to test purely repulsive behaviour for a variety of exponents.

$$\phi(r) = \frac{\lambda_r}{\lambda_r - \lambda_a} \left(\frac{\lambda_r}{\lambda_a} \right)^{\frac{\lambda_r}{\lambda_r - \lambda_a}} \epsilon \left(\left(\frac{\sigma}{r} \right)^{\lambda_r} - \left(\frac{\sigma}{r} \right)^{\lambda_a} \right) - \phi_{Mei}(r_c) \quad (4)$$

This form can be used to mimic the discontinuous potential of an idealised hard-sphere system.²

- DVLO-type potentials

$$\phi(r) = \epsilon \left(\alpha \left(\frac{\sigma}{r} \right)^{12} - \left(\frac{\sigma}{r} \right)^8 + \left(\frac{\sigma}{r} \right)^4 \right) \quad (5)$$

$$\phi(r) = \epsilon_h \left(\frac{\sigma}{r + \delta} \right)^{12} - \epsilon_h \left(\frac{\sigma}{r + \delta} \right)^8 + \epsilon_w \frac{\sigma \exp(-\kappa(r + \delta - 1)^4)}{r + \delta} \quad (6)$$

These two potentials are invented potentials designed to try and mimic the secondary stable minimum seen in DVLO theory.

Core-Softened Potentials:

- Smooth Step Potential

$$\phi(r) = \epsilon_h \left(\frac{\sigma}{r} \right)^{12} + \frac{\epsilon_s}{1 + \exp[2\kappa(r - \delta)]} \quad (7)$$

Current closure relationships are known to fail for systems with features over multiple length scales making the smooth step a good choice of training system if we want to extend the generalisability of our inferred closure.

- Continuous Shouldered Well (CSW)

$$\phi(r) = \epsilon_h \left(\frac{\sigma}{r} \right)^{12} + \frac{\epsilon_s}{1 + \exp[2\kappa(r - \delta_s)]} - \epsilon_w \exp \left(-\frac{1}{2} \left(\frac{r - \delta_g}{\chi} \right)^2 \right) \quad (8)$$

The CSW model is a core-softened model in the same manner as the smooth step but it has also been shown to recreate physical anomalies seen experimentally in fluids such as water.³

- Repulsive Shoulder System Attractive Well (RSSAW)

$$\phi(r) = \epsilon_h \left(\frac{\sigma}{r} \right)^{14} + \lambda_0 - \lambda_1 \tanh(k_1[r - \sigma_1]) + \lambda_2 \tanh(k_2[r - \sigma_2]) \quad (9)$$

The RSSAW model is similar to the CSW model and exhibits the same complex behaviour.⁴ The potentials of this form have been reported for colloidal particles and polymer-colloid mixtures making them important for the study of soft matter systems.

Soft-Sphere Potentials:

- Soft-Sphere

$$\phi(r) = \epsilon \left(\frac{\sigma}{r} \right)^n \quad (10)$$

The soft-sphere potential is purely repulsive but allows for more interpenetration than other repulsive models.

- Yukawa

$$\phi(r) = \epsilon \frac{\sigma \exp(-\kappa r)}{r} \quad (11)$$

The Yukawa potential is a screened coulomb potential that is used to represent the effect of charges in ionic solutions.

Soft-Core Potentials:

- Hertzian

$$\phi(r) = \epsilon \left(1 - \frac{r}{r_c}\right)^{5/2} \quad (12)$$

The Hertzian potential effectively describes the interactions between weakly deformable bodies such as globular micelles. Soft-core potentials are qualitatively different from soft-sphere potentials in far as complete overlap is allowed.

- Hat

$$\phi(r) = F_{max} \cdot \frac{r - r_c}{\sigma} \cdot \left(\frac{r + r_c}{2r_c} - 1\right) \quad (13)$$

The Hat potential is a standard conservative potential often used in Dissipative Particle Dynamics for simulating coarse grained fluids.

- Gaussian

$$\phi(r) = \epsilon \exp\left(-\frac{1}{2} \left(\frac{r}{\sigma}\right)^2\right) \quad (14)$$

Gaussian shaped potentials have been used as reasonable approximations for the effective interaction between the centres of polymer chains (Flory-Krigbaum potential⁵).

Simulation Details

ESPREsSo is a highly flexible open source Molecular Dynamics package designed for the simulation of soft matter systems. The simulation engine is written in C and C++ but is controlled via a Python interface.

Interaction potentials were specified using regularly spaced tabulated values, these are linearly interpolated in the core to evaluate the forces at each time step.

For each state point investigated the density was specified and the box size was fixed at 20σ where σ is the scale parameter of the density. The number of particles under consideration was scaled accordingly.

The system is integrated using the Velocity Verlet algorithm.^{6,7} The resulting global errors in the velocities and positions are $O(\Delta t^2)$. In setting the time step we want use the maximum time step possible that yields sufficient accuracy for this purpose a time step of $\Delta t = 0.005$ has been used.

A Langevin thermostat is used to control the system temperature. The Langevin thermostat introduces stochastic momentum fluctuations that both regulate the temperature and are necessary to recreate the fluctuations observed in the canonical ensemble (NVT) making it superior to a rescaling thermostat that would suppress such fluctuations.

In order to minimise the chances of a quasi-stable solid state forming particle positions are randomly initialised to ensure a low symmetry starting arrangement. At the start of each simulation run a static energy minimisation is performed via gradient descent without the thermostat to remove any overlaps present between hard-sphere potentials. Burn-in runs were then carried out with the thermostat to allow the system to equilibrate. Equilibrium was taken to be the point at which the kinetic temperature over a short windowing period is consistent with the reference temperature of the thermostat.

For computational efficiency the potentials used are truncated at $r_{cut} = 3$. The potentials have also been adjusted to fix the potential and force at the cut-off. Often this treated with caution as it introduces systematic errors when measuring the thermodynamic properties of

a reference system. However, as the structural correlation functions are causally determined by Newton’s laws their validity is unaffected by adjusting the potential. Verlet lists are used to efficiently handle the truncation of the potential. A skin length of 0.2 times the cut-off length was chosen in line with common practise.⁸

The radial distribution function and structure factor were measured from the simulation. To get the structure factor in a timely manner we only take measurements along {100} type directions within the system such that evaluating $S(q)$ is $O(N)$ in the number of particles. The default approach that evaluates $S(q)$ for every valid grid point scales as $O(N^3)$. In total for each state point 1024 samples were taken at intervals of 16 time steps. The variances were handled using the Flyjberg-Peterson blocking approach.⁹

Reliable calculation of the Direct Correlation function

The direct correlation function, $c(r)$, can be evaluated from measurements of the static structure factor, $S(q)$, based of the relationship that:

$$C(r) = iFT\left(\frac{1}{\rho}\left(1 - \frac{1}{S(q)}\right)\right) \quad (15)$$

In simulation studies the most common approach for calculating the $S(q)$ is taking the Fourier transform of the total correlation function.

$$S(q) = 1 + \frac{4\pi\rho}{q} \int_0^\infty h(r)r \sin(qr) dr \quad (16)$$

However, the minimum image convention means $h(r)$ can only be measured up to half the box length. This limit truncates the domain of the Fourier transform leading to finite size effects. Of the possible finite size effects incurred by truncation the most significant is that the apparent $S(q)$ is not guaranteed to be non-negative in the limit $q \rightarrow 0$.¹⁰ These artefacts result in large-amplitude long-wavelength fluctuations in $c(r)$ that are inconsistent

with the limiting behaviour $\lim_{r \rightarrow \infty} c(r) \simeq -\beta\phi(r)$.

In previous work approximate extension schemes¹¹ have been used to extend $h(r)$ to infinity to avoid such issues. However, such extension schemes the rely on the use of a pre-determined closure. The other approach is to calculate $S(q)$ directly from the Fourier transform of the density. However, this approach is computationally much more expensive and is subject to significant noise in the expected value of $S(q)$ for high wave vectors resulting in short-wavelength fluctuations in $c(r)$.

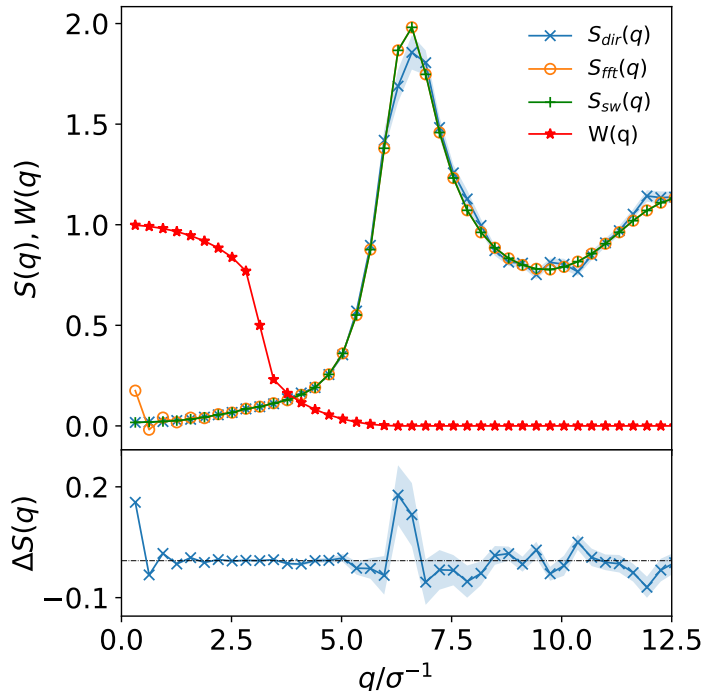


Figure 1: The upper section shows $S(q)$ as determined directly and from the Fourier transform and shows how the two results are joined together using the switching function $W(q)$. The lower section is a detail of the difference between the direct and Fourier methods for calculating $S(q)$. The figure clearly shows the large oscillations in the low q limit that our method helps to tackle but example also shows the deviation around the principle peak in $S(q)$ which our approach fails to address in some cases.

In this work to avoid both of these limitations we opt for a Poisson re-summation inspired approach where we evaluate $S(q)$ directly for small wavelengths and from the Fourier transform of $h(r)$ for large wavelengths. A smooth cosine switching function is used to blend

between the two regimes. This approach ensures we get the correct limiting behaviour in the $q \rightarrow 0$ limit for high density systems suppressing the non-physical artefacts that would otherwise be observed in $c(r)$ if a naive approach was adopted. However, this approach does come with its own limitations as we need to define the switching point heuristically. To reduce potential artefacts from the switching operation we place the transition point in the region before the principle peak where the best agreement is observed between the two methods of calculating $S(q)$. However, for several systems (Figure 1) we observed deviations between the direct and Fourier transform results around the principle peak which in turn can lead to comparatively small but still undesirable intermediate wavelength fluctuations in $c(r)$.

Heuristic data cleaning

The Ornstein-Zernike formalism is only valid for liquid state systems. Given the high-throughput approach used to generate data it is necessary to identify and exclude solid, two-phase and non-equilibrium samples before it can be used. This is done using several physically motivated heuristics. The Hansen-Verlet criterion,¹² $S(q_{peak}) > 2.8$, is used to identify solid and two phase solid-liquid samples. Gaseous and two-phase liquid-gas systems are identified using the heuristic criteria that $S(0) > 1$. This criteria is derived by noting that the compressibility of a system is given by:

$$S(q \rightarrow 0) = \rho k_b T \kappa_T \tag{17}$$

As gases are typically characterised by their highly compressible nature and noting that for an uncorrelated liquid $S(0) \simeq 1$ we propose that divergence of $S(q)$ in the limit $q \rightarrow 0$ is indicative of gaseous and two-phase liquid-gas behaviour. In total 450 out of 480 potential systems investigated passed these heuristic criteria.

Mixture Coarse Graining Details

The downstream test of the learnt closure on coarse graining task made use of 2 species of Lennard-Jones particle that interacted with each other via another Lennard-Jones type potential.

The energy scales were $\epsilon_{00} = 1.0$, $\epsilon_{01} = 1.1$, and $\epsilon_{11} = 1.0$, the length-scale were $\sigma_{00} = 1.0$, $\sigma_{01} = 0.75$, and $\sigma_{11} = 0.5$. The cutoff distances were $R_{00}^{cut} = 2.5$, $R_{01}^{cut} = 2.5$, and $R_{11}^{cut} = 1.5$. The rest of the simulations details were exactly as described above.

The quadratic Savitzky-Golay filter used to smooth the bridge function to obtain well behaved forces used window size of 21.

References

- (1) Weeks, J. D.; Chandler, D.; Andersen, H. C. Role of Repulsive Forces in Determining the Equilibrium Structure of Simple Liquids. *The Journal of Chemical Physics* **1971**, *54*, 5237–5247, DOI: 10.1063/1.1674820.
- (2) Jover, J.; Haslam, A.; Galindo, A.; Jackson, G.; Müller, E. Pseudo hard-sphere potential for use in continuous molecular-dynamics simulation of spherical and chain molecules. *The Journal of Chemical Physics* **2012**, *137*, 144505.
- (3) Lukšič, M.; Hribar-Lee, B.; Pizio, O. Phase behaviour of a continuous shouldered well model fluid. A grand canonical Monte Carlo study. *Journal of molecular liquids* **2017**, *228*, 4–10.
- (4) Fomin, Y. D.; Tsiok, E.; Ryzhov, V. Complex phase behavior of the system of particles with smooth potential with repulsive shoulder and attractive well. *The Journal of chemical physics* **2011**, *134*, 044523.
- (5) Flory, P. J.; Krigbaum, W. R. Statistical Mechanics of Dilute Polymer Solutions. II. *The Journal of Chemical Physics* **1950**, *18*, 1086–1094, DOI: 10.1063/1.1747866.

- (6) Verlet, L. Computer "Experiments" on Classical Fluids. I. Thermodynamical Properties of Lennard-Jones Molecules. *Phys. Rev.* **1967**, *159*, 98–103, DOI: 10.1103/PhysRev.159.98.
- (7) Swope, W. C.; Andersen, H. C.; Berens, P. H.; Wilson, K. R. A computer simulation method for the calculation of equilibrium constants for the formation of physical clusters of molecules: Application to small water clusters. *The Journal of Chemical Physics* **1982**, *76*, 637–649, DOI: 10.1063/1.442716.
- (8) Frenkel, D.; Smit, B. *Understanding Molecular Simulation*; Academic Press, Inc., 2001.
- (9) Flyvbjerg, H.; Petersen, H. G. Error estimates on averages of correlated data. *The Journal of Chemical Physics* **1989**, *91*, 461–466.
- (10) Frenkel, D. Simulations: The dark side. *The European Physical Journal Plus* **2013**, *128*, 10, DOI: 10.1140/epjp/i2013-13010-8.
- (11) Jolly, D. L.; Freasier, B. C.; Bearman, R. J. The extension of simulation radial distribution functions to an arbitrary range by baxter's factorisation technique. *Chemical Physics* **1976**, *15*, 237 – 242, DOI: [https://doi.org/10.1016/0301-0104\(76\)80156-5](https://doi.org/10.1016/0301-0104(76)80156-5).
- (12) March, N.; Tosi, M. *Introduction to Liquid State Physics*; World Scientific, 2002.